Inorganic Chemistry

Article

pubs.acs.org/IC

Turning a New Leaf on Metal-TMC Chemistry: Ni^{II}(TMC) Acetylides

Sarah F. Tyler,[†] Sean N. Natoli,[†] Bess Vlaisavljevich,[‡] Phillip E. Fanwick,[†] and Tong Ren*[,†]

[†]Department of Chemistry, Purdue University, West Lafayette, Indiana 47907, United States

[‡]Department of Chemical & Biomolecular Engineering, University of California, Berkeley, California 94720, United States

Supporting Information

ABSTRACT: Novel [Ni(TMC)C≡CY]$^+$-type compounds **1**−**4** [TMC = 1,4,8,11-tetramethyl-1,4,8,11-tetraazacyclotetradecane; Y = $SiMe_3$ (**1**), Si^iPr_3 (**2**), Ph (**3**), and C_2H (**4**)] have been synthesized and characterized. Single-crystal X-ray diffraction studies revealed that these compounds adopt a distorted square-pyramidal geometry, with the acetylide ligand occupying the apical position and a *RSRS* isomer for the TMC ligand. The room temperature magnetic properties of **1**−**4** are consistent with an S = 1 ground state, as corroborated by CASSCF and density functional theory calculations, which indicate that the singly occupied molecular orbitals are d_{z^2} and $d_{x^2-y^2}$.

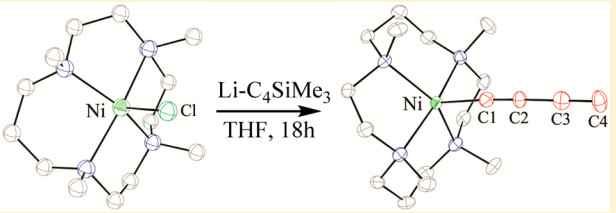

INTRODUCTION

The coordination chemistry of the macrocyclic ligand 1,4,8,11-tetramethyl-1,4,8,11-tetraazacyclotetradecane (TMC) has been studied extensively since its discovery in 1973.[1−3] The coordination chemistry of TMC covers a broad range of transition metals including iron, ruthenium, platinum, copper, manganese, and cobalt.[2] The modeling of dioxygen activation by nonheme metalloenzymes based on TMC compounds has been a recent focus.[4] In comparison, the organometallic chemistry of Ni(TMC) has been less studied and is of interest to us. Fascinating examples of organic transformations facilitated by Ni(TMC) species include stoichiometric reactions between [Ni(TMC)]$^+$ and disubstituted alkanes to produce alkenes,[5] reductive dehalogenation of 1,3-dichloropropane catalyzed by [Ni(TMC)]$^{2+}$ immobilized in Nafion,[6] and electrocatalytic cyclization of bromoalkoxylated derivatives by [Ni(TMC)]$^+$.[6,7] Notably, Ni(TMC) has also been of use in biomimetic studies,[8] including the organometallic complex [Ni(TMC)CH_3]$^+$ as a functional mimic of acetyl-CoA.[9−11]

Curiously, transition-metal acetylide compounds with TMC as the auxiliary ligand remain unknown to date. Building on the earlier successes in the chemistry of diruthenium acetylides,[12] our laboratory staff has explored the synthesis and properties of acetylide compounds based on 3d metal cyclam (cyclam = 1,4,8,11-tetraazacyclotetradecane) motifs with Cr^{III},[13] Fe^{III}[14] and Co^{III} metal centers.[15] It is thus of interest to extend the alkynylation chemistry to metal-TMC [M(TMC)] compounds, and nickel is an appealing choice because of the variety of coordination chemistry for Ni^{II}(TMC).[3,4,16,17]

The chemistry of nickel acetylides has a long history and dates back to the synthesis of [Ni(C≡CR)$_4$]$^{2-}$ by Nast in the 1950s.[18] Humphrey and co-workers explored a variety of nickel acetylides as second- and third-order nonlinear-optical chromophores.[19] Cotton et al. reported several examples of the Ni_3(dpa)$_4$-type compounds (dpa = 2,2′-dipyridylamide) bearing axial arylacetylide ligands.[20] Other recent examples include explorations of the reactivity of nickel acetylides toward the electron acceptor 7,7,8,8-tetracyanoquinodimethane,[21] their catalytic alkyne polymerization,[22] and catalytic cross-couplings between alkyl halides and alkynyl Grignard reagents.[23] Described herein are the preparation and characterization of the first examples of transition-metal-TMC acetylide compounds, Ni(TMC) acetylides **1**−**4** (Scheme 1). These compounds are also the only examples of Ni^{II}(TMC) organometallic derivatives since the initial report of [Ni(TMC)CH_3]$^+$ by D'Aniello and Barefield.[16]

Scheme 1. Synthesis of Ni^{II}(TMC) Acetylides

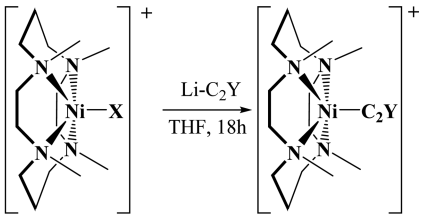

X = Cl$^-$, OTf$^-$; Y = $SiMe_3$ (**1**), Si^iPr_3 (**2**), Ph (**3**) and C_2H (**4**)

RESULTS AND DISCUSSION

As shown in Scheme 1, monoacetylide compounds **1**−**4** were prepared from the reaction between [Ni(TMC)Cl]Cl[24] and the appropriate lithium acetylide. Compounds **1** and **2** were prepared using 3 equiv of LiC_2SiMe_3 and $LiC_2Si^iPr_3$ and isolated as mint-green powders in yields of 45% and 78%, respectively. Compound **3** was prepared using 2.4 equiv of LiC_2Ph and isolated as a mint-green powder in a yield of 60%. Compound **4** was prepared from 2.1 equiv of LiC_4SiMe_3 and

Received: August 17, 2015
Published: September 28, 2015

DOI: 10.1021/acs.inorgchem.5b01883
Inorg. Chem. 2015, 54, 10058−10064

isolated as an emerald-green powder in a yield of 61%. In some instances, [Ni(TMC)OTf]OTf[24] (OTf = trifluoromethanesulfonate) was used as the starting material for easier purification and crystallization, which led to the isolation of compounds with a OTf counterion (**1b** and **4b**). When a stoichiometric amount of lithium reagent was used, a substantial amount of unreacted starting material was detected by electrospray ionization mass spectrometry (ESI-MS) in the reaction mixture. Additional lithium reagent was added until complete consumption of the starting material, as indicated by ESI-MS. It is worth noting that the use of *n*-BuLi or lithiated acetylide in significant excess would lead to the displacement of nickel from TMC, with both Li(TMC) and free TMC being the predominant species in ESI-MS, and result in less or no product. All [Ni(TMC)(C_2R)]X compounds appear to be stable indefinitely under ambient conditions. Room temperature magnetic susceptibility measurements of solid samples yielded effective magnetic moments of 2.94, 2.83, 2.97, and 2.75 μ_B for compounds **1**−**4**, respectively, which are consistent with a high-spin Ni^{II} center (S = 1). All compounds were authenticated using both ESI-MS and elemental analysis.

Compounds **1**−**4** crystallize readily via slow diffusion of a nonpolar solvent into a tetrahydrofuran (THF) or CH_2Cl_2 solution, and compounds **2**−**4** were further characterized with single-crystal X-ray diffraction. Cations $\mathbf{2}^+$ and $\mathbf{3}^+$ were crystallized as the chloride salts, while cation $\mathbf{4}^+$ was crystallized with a triflate ion (**4b**). In each of the three cases, the asymmetric unit contains an independent molecule. The molecular structures of $\mathbf{2}^+$, $\mathbf{3}^+$, and $\mathbf{4}^+$ are shown in Figures 1−3, respectively, and the selected bond lengths and angles are collected in Table 1.

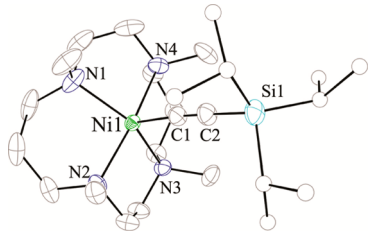

Figure 1. ORTEP plot of $\mathbf{2}^+$ at the 30% probability level. H atoms were omitted for clarity.

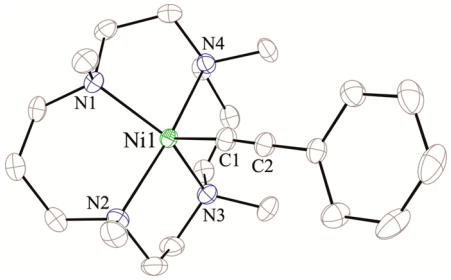

Figure 2. ORTEP plot of $\mathbf{3}^+$ at the 30% probability level. H atoms were omitted for clarity.

All three cations exhibit Ni−N bond lengths of ca. 2.15 Å, which are comparable to those of [Ni(TMC)Cl]Cl[24] and [Ni(TMC)CH_3](BArF)(BArF$^-$ = [B(3,5-$(CF_3)_2C_6H_3)_4$]$^-$).[10] The Ni−C1 bond of $\mathbf{4}^+$ [2.001(7) Å] is slightly elongated from those of $\mathbf{3}^+$ [1.985(2) Å] and $\mathbf{2}^+$ (1.975 Å). All three cations have shorter Ni−C bonds than that found for [Ni(TMC)-CH_3]$^+$ [2.04(1) Å],[10] and the shortening is due to the difference between *sp*-C and sp^3-C. The C≡C bond lengths in $\mathbf{2}^+$−$\mathbf{4}^+$ fall within the expected range for triple bonds.[25]

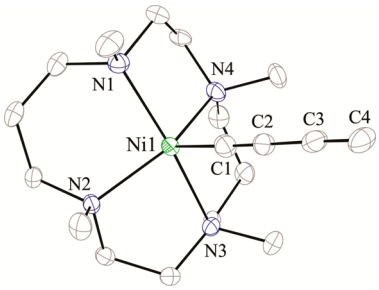

Figure 3. ORTEP plot of $\mathbf{4}^+$ at the 30% probability level. H atoms were omitted for clarity.

Table 1. Selected Bond Lengths (Å) and Bond Angles (deg) for $\mathbf{2}^+$, $\mathbf{3}^+$, and $\mathbf{4}^+$

	$\mathbf{2}^+$	$\mathbf{3}^+$	$\mathbf{4}^+$
Ni1−C1	1.975(3)	1.985(2)	2.000(6)
Ni1−N1	2.111(3)	2.1068(2)	2.160(5)
Ni1−N2	2.161(3)	2.2034(2)	2.128(4)
Ni1−N3	2.112(3)	2.1324(2)	2.193(5)
Ni1−N4	2.189(3)	2.1623(2)	2.133(5)
C1−C2	1.187(5)	1.192(3)	1.189(8)
C2−C3			1.389(8)
C3−C4			1.190(9)
Ni1−C1−C2	176.6(3)	175.0(2)	176.6(6)
C1−Ni1−N1	109.64(2)	110.83(8)	95.2(2)
C1−Ni1−N2	94.38(1)	93.64(8)	109.5(2)
C1−Ni1−N3	105.97(1)	104.75(9)	94.9(2)
C1−Ni1−N4	95.43(1)	95.94(8)	104.9(2)
N1−Ni1−N3	144.40(1)	144.40(7)	169.94(2)
N2−Ni1−N4	170.18(1)	170.42(7)	145.58(2)

As shown in Figures 1−3, the coordination spheres of the Ni^{II} center in $\mathbf{2}^+$−$\mathbf{4}^+$ are best described as a square pyramid, with four N centers occupying the basal positions and the acetylide assuming the apical position. The square pyramid appears to be distorted toward trigonal-bipyramidal geometry upon close examination of the N−Ni−N angles. The degree to which the Ni center is "buckled" out of the TMC ring can be gleaned from the N1−Ni−N3 and N2−Ni−N4 angles in each compound (Scheme 2c). For instance, the Ni center in $\mathbf{2}^+$ is displaced by roughly 0.65 Å with respect to N1 and N3 (N1−Ni−N3 of ca. 144°) and 0.19 Å with respect to N2 and N4 (N2−Ni−N4 of ca. 170°), resulting in an average displacement

Scheme 2. Depiction of the Dihedral Angles in the Equatorial (Edges e_1−e_3, a) and Axial (Edges a_1-a_6, b) Positions Used To Determine the Geometry of $\mathbf{2}^+$−$\mathbf{4}^+$ (a and b) and Calculation of the Buckling Seen for the Ni Center with Respect to N1−N3 and N2−N4 (c)

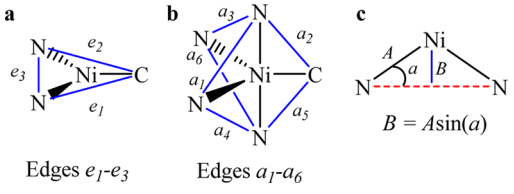

DOI: 10.1021/acs.inorgchem.5b01883
Inorg. Chem. 2015, 54, 10058−10064

of 0.42 Å. Similarly, the Ni center in $3^+/4^+$ is displaced by approximately 0.65/0.19 Å with respect to N1 and N3 and 0.18/0.63 Å with respect to N2 and N4.

In order to determine the degree to which the distortion favored either geometry, the structures were further analyzed using the method of Meutterties and Guggenberger.[26] To use this method, the dihedral angles of a complex are compared to known compounds that span the Berry rearrangement pathway ($D_{3h} \rightarrow C_{4v}$); from the comparison, one can deduce where a complex falls within the pathway. The dihedral angles used are indicated by the line of intersection between two planes, as shown in Scheme 2a,b. The dihedral angles of 2^+–4^+ are given in Table 2, as are those for an ideal square pyramid and an ideal trigonal bipyramid, while complexes that span the full pathway can be found in ref 26. The dihedral angles gathered suggest that the geometry of 2^+–4^+ is neither an ideal trigonal bipyramid nor a square pyramid but rather falls in the middle of the Berry rearrangement pathway. This conclusion is further validated using the technique of Addison and co-workers, in which they defined the geometric parameter τ (eq 1, where α is the smallest N1/2–Ni–N3/4 angle and β is the largest N1/2–Ni–N3/4 angle) as an index for the degree of distortion between the trigonal-bipyramidal ($\tau = 1$) and square-pyramidal ($\tau = 0$) geometries.[27] The values of τ for 2^+–4^+ are 0.43, 0.43, and 0.41.

Table 2. Dihedral Angles (deg) for 2^+–4^+, an Ideal Square Pyramid, and an Ideal Trigonal Bipyramid[26]

	2^+	3^+	4^+	ideal square pyramid	ideal trigonal bipyramid
e_1	63.46	64.37	62.12	75.7	53.1
e_2	61.59	60.47	64.85	75.7	53.1
e_3	23.99	24.25	23.03	0.0	53.1
a_1	113.61	113.23	113.72	119.8	101.5
a_2	94.57	94.14	95.48	75.7	101.5
a_3	113.03	113.61	113.8	119.8	101.5
a_4	111.93	111.12	116.22	119.8	101.5
a_5	94.50	94.70	95.16	75.7	101.5
a_6	115.98	116.28	111.61	119.8	101.5

$$\tau = \frac{\beta - \alpha}{60} \quad (1)$$

The stereoisomer of the TMC ligand also merits a brief comment: the *RSRS* isomer is established unambiguously for compounds **2**–**4** reported herein (see Scheme 1 and Figures 1–3), as well as for the nickel(II) compounds developed by Tatsumi et al.[24,28] In contrast, $[Ni(TMC)CH_3]^+$, exists as a 60:40 mixture of the *RSRS* and *RRSS* isomers in the solid state.[10] Like cyclam complexes, M(TMC) complexes have five possible stereoisomers, as shown in Scheme 3, with the most common stereoisomer for TMC being *RSRS*. The introduction of the methyl groups leads to steric strain within the ligand, causing it to "buckle", which has been shown to sterically shield a fifth ligand in M(TMC) complexes, thereby increasing the complexes' stability.[3,4]

The UV–vis spectra of **1** and **2** are quite similar, and both exhibit two d–d transition peaks (between 400 and 450 nm and at 650–700 nm), as shown in Figure 4. Compounds **3** and **4** also exhibit two d–d transitions, albeit the higher energy d–d bands appear as shoulders instead. The appearance of two d–d transitions in all four compounds is consistent with the spectral

Scheme 3. TMC Stereoisomers as Adapted from Reference 2

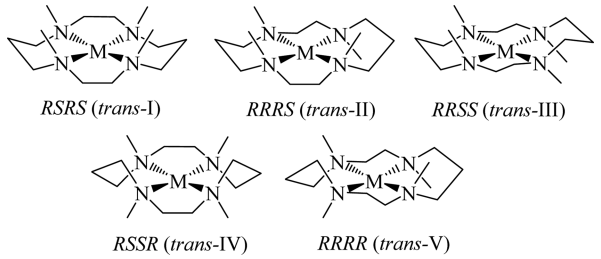

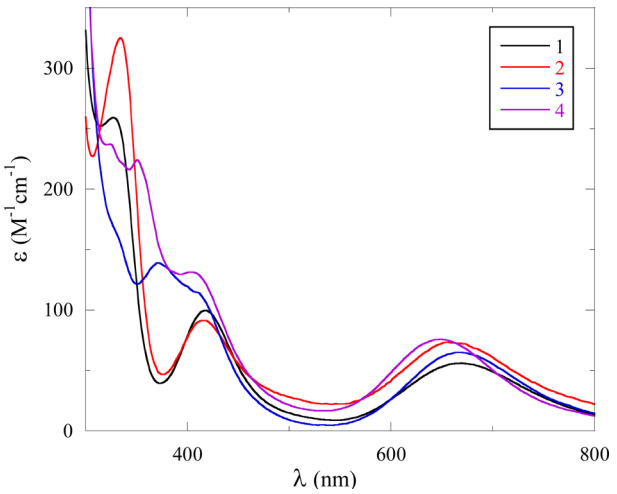

Figure 4. UV–vis absorption spectra of compounds **1**–**4** in CH_2Cl_2.

characteristics noted for the precursor compound [Ni(TMC)Cl]Cl (423 and 707 nm).[24] Similar to $[Ni(TMC)CH_3](BArF_4)$,[11] the transition observed below 400 nm for **1** and **2** is likely attributed to the $\sigma(C) \rightarrow \sigma(Ni)$ charge transfer. Complexes **3** and **4** also exhibit the $\sigma(C) \rightarrow \sigma(Ni)$ charge transfer with additional shoulders. Although not shown in Figure 4, all four compounds exhibit an intense peak ($\varepsilon > 10^3$ M^{-1} cm^{-1}) below 300 nm that is assigned to the N → Ni charge-transfer band.[11]

The redox activity of compounds **1**–**4** was examined with cyclic voltammetry measurements, and the results for compounds **1**–**4** and [Ni(TMC)Cl]Cl are shown in Figure 5. All four compounds display an irreversible one-electron reduction attributed to the $Ni^{II/I}$ couple (A), as well as a broad, irreversible one-electron oxidation assigned as the $Ni^{III/II}$ couple (B). The one-electron reduction remains irreversible with scan rates up to 1 V s^{-1} (Figure S1 in the Supporting Information), indicating a fast chemical step upon reduction. The A couple of compounds **1**–**4** appears in a narrow range from −1.89 to −1.99 V. Interestingly, the A couple in compound **4** is anodically shifted to −1.78 V because butadiynyl is more electron-deficient than ethynyl, in agreement with the structural data. In comparison, [Ni(TMC)Cl]Cl displays a (quasi)reversible reduction at −1.35 V, and, likewise, $[Ni(TMC)CH_3]^+$ exhibits a (quasi)reversible reduction at −1.0 V (vs Ag/AgCl).[10] The cathodic shift of the electrode potentials for acetylide compounds is clearly attributed to the increase in the σ donation upon going from a chloro to an acetylide apical ligand (Table 3). The cause of the irreversibility is unclear to us.

In order to further understand the electronic structures of Ni(TMC) acetylide complexes, spin-unrestricted density func-

DOI: 10.1021/acs.inorgchem.5b01883
Inorg. Chem. 2015, 54, 10058–10064

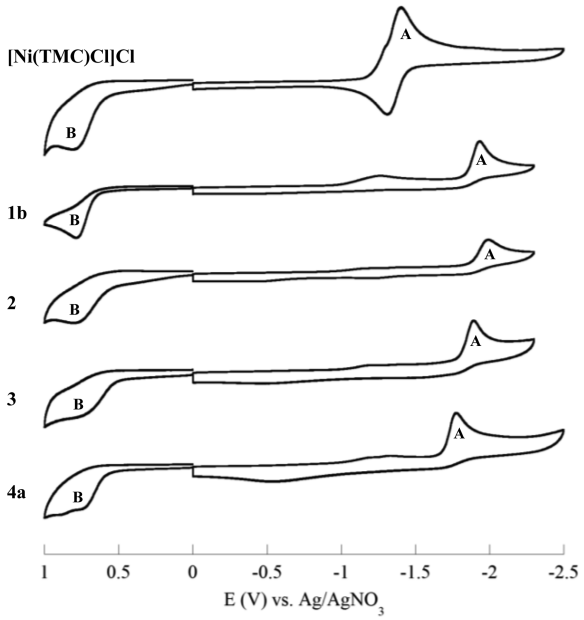

Figure 5. Cyclic voltammograms recorded for [Ni(TMC)Cl]Cl and compounds **1**−**4** in a 0.20 M Bu_4NPF_6/acetonitrile solution at a scan rate of 100 mV s^{-1}. The triflate salt of **1** (**1b**) was used because of the solubility issue; chloride salts were used for the other compounds.

Table 3. Electrode Potentials (V) for [Ni(TMC)Cl]Cl and 1−4

	E_{pa}(B)	E_{pc}(A)
[Ni(TMC)Cl]Cl	0.81	−1.35
1b	0.87	−1.93
2	0.80	−1.99
3	0.71	−1.89
4a	0.75	−1.78

tional theory (DFT) calculations were performed at the B3LYP/LanL2DZ level using the *Gaussian03* software package.[29] Geometry optimizations were performed for the cationic compounds $\mathbf{2}^+$−$\mathbf{4}^+$ in the S = 1 ground state using the X-ray structures of **2**−**4** as the starting point. Structures were confirmed as minima by means of harmonic vibrational analysis. For compound $\mathbf{2}^+$, the −$SiMe_3$ moiety on the acetylide was replaced with −H. DFT-optimized structures will be referred to as **2′**−**4′**. Additionally, complete active space self-consistent-field calculations with corrections from second-order perturbation theory (CASSCF/CASPT2)[30] were performed for **4′** to ensure that additional electronic states were not contributing to the ground state, particularly configurations involving excitations onto the butadiynyl group.

The optimized bond lengths within the nickel coordination spheres of **2′**−**4′** are in good agreement with those from the crystal structures. The average Ni−N bond length is slightly elongated to approximately 2.21 Å in all three models. The C≡C bond lengths are elongated to approximately1.24 Å for **2′** and **3′** and 1.25/1.23 Å (C1−C2/C3−C4) for **4′**. The Ni center is also slightly more buckled for **2′**/**3′**/**4′** by 0.68 Å/0.70 Å/0.20 Å with respect to N1/N3 and by 0.21 Å/0.23 Å/0.68 Å with respect to N2/N4 but is consistent with the geometry seen in the crystal structures. Deviations of this magnitude are expected given that crystal-packing effects were not accounted for in our DFT optimization.

Selected frontier molecular orbitals (MOs) for **2′**−**4′** are shown in Figure 6a−c, respectively. The singly occupied molecular orbitals SOMO and SOMO−1 are dominated by contributions from the $d_{x^2-y^2}$ and d_{z^2} orbitals, respectively, as one would expect for a d^8 ion in a square-pyramidal geometry. As seen in Figure 6, the SOMOs for **4′** are more stabilized than those for **2′** and **3′**, as is expected with the increase in the acetylenic units; this is in agreement with the anodic shift in the reduction potentials from **1**−**3** to **4**. While HOMO−2 and HOMO−3 of **2′** and **4′** contain the contributions from the linear combinations of d_{yz} and d_{xz}, they are dominated by the π(C≡C) orbitals of the butadiyne. Note that HOMO−3 for **3′** only shows a contribution from a π orbital that is localized on the phenyl ring, and there is no metal contribution. HOMO−2 and HOMO−4 for **3′**, however, follow the same trend as that seen for HOMO−2 and HOMO−3 of **2′** and **4′**. The d_{yz}/d_{xz} and π(C≡C) orbitals are of opposite signs, consistent with the fact that π interactions in metal acetylides are primarily of the filled−filled type.[31] The MOs with dominant d_{xy}, d_{yz}, and d_{xz} character are not included in the frontier MOs shown in Figure 6 because they lie lower in energy.

Furthermore, we have performed high-level CASSCF/CASPT2 calculations, and these results are consistent with DFT. CASSCF is a multiconfigurational method, and as such more than one electron configuration is considered at the same time (see ref 31 for a further explanation of the method).[32,33] For **4′**, the active space includes the π_g and π_u orbitals (four orbitals) and their antibonding pairs (four orbitals) on the acetylide along with the five 3d orbitals for a total of 13 orbitals (see Figure 7). The corresponding number of electrons in the active space is 16 because of the Ni^{II} d^8 metal and the four doubly occupied π orbitals. By comparing Figures 6c and 7, we can see that the SOMOs are localized on the metal center in both cases. Additionally, the set of orbitals immediately under the SOMOs are the π_u orbitals. In the CASSCF calculation, this set of orbitals has a lower occupation number, indicating that these orbitals are "less occupied" than the π_g orbitals, which correlates with the orbitals being higher in energy. Therefore, the CASSCF results yield the same description as DFT, which is not particularly surprising because the $\pi_u^4\pi_u^4d^2$ electronic configuration contributes 87% to the total wave function (all other configurations contribute less than 1% each). As in DFT, the d_{xy} orbital lies very low in energy and consequently does not remain in the active space following orbital optimization.

■ CONCLUSION

The successful synthesis of new compounds **1**−**4** revealed the feasibility of alkynylation chemistry of Ni(TMC), which affords monoacetylide selectively. In comparison, the acetylide chemistry of M(cyclam) is dominated by the formation of bis-acetylides. Given the abundance of both [M(TMC)X]X and $M(TMC)X_2$ (M = 3d metal; X = halide) type compounds, the potential to extend the synthetic chemistry developed here to compounds based on other 3d metals or structurally sophisticated acetylides is unlimited, and a further investigation is currently underway.

■ EXPERIMENTAL SECTION

General Procedures. Phenylacetylene, (triisopropylsilyl)-acetylene, (trimethylsilyl)acetylene, and 1,4-bis(trimethylsilyl)-butadiyne were purchased from GFS Chemicals. 1,4,8,11-Tetraazacyclotetradecane was purchased from Matrix Scientific, from which 1,4,8,11-tetramethyl-1,4,8,11-tetraazacyclotetradecane (TMC) was

DOI: 10.1021/acs.inorgchem.5b01883
Inorg. Chem. 2015, 54, 10058−10064

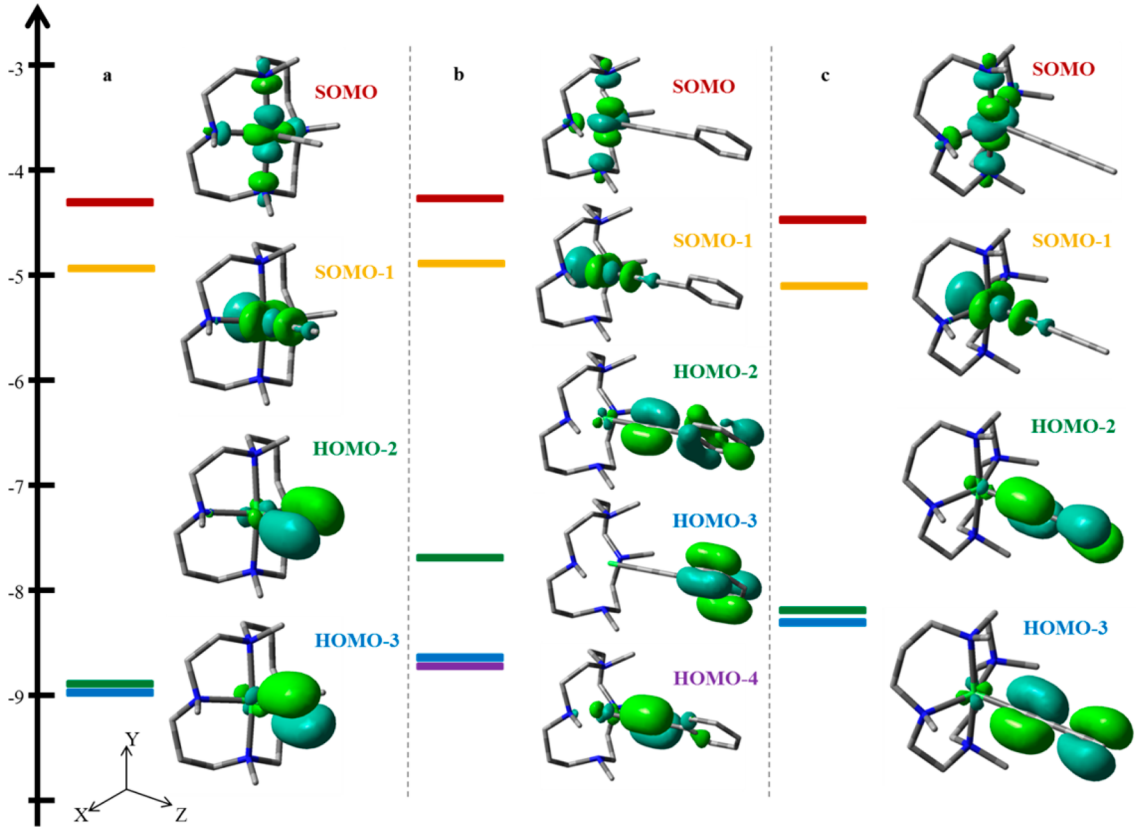

Figure 6. Frontier MO diagrams obtained from DFT calculations at an isovalue of 0.05 for (a) **2′**, (b) **3′**, and (c) **4′**.

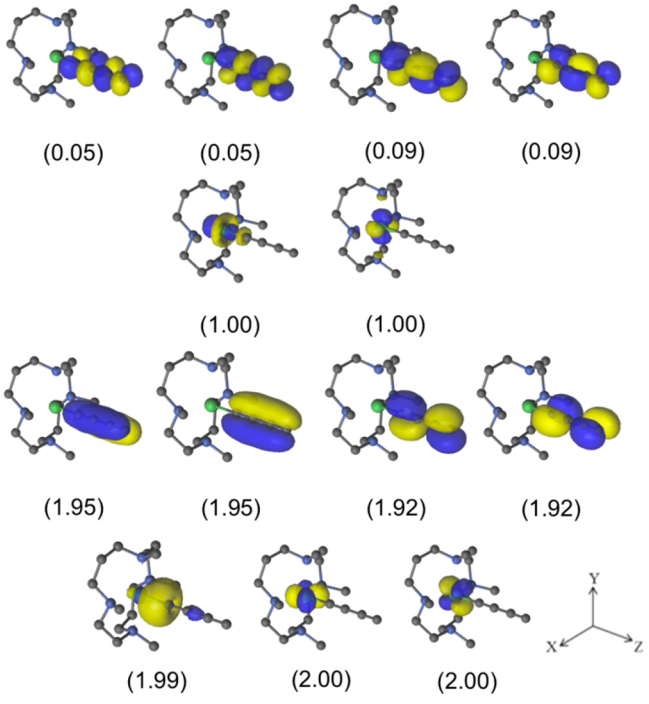

Figure 7. Active natural orbitals and corresponding occupation numbers from the (16,13) CASSCF calculation for **4′**.

prepared according to the literature procedure.[1] Nickel starting materials [Ni(TMC)Cl]Cl and [Ni(TMC)(OTf)](OTf) were prepared using the literature procedure.[1,24] Tetrahydrofuran (THF) was freshly distilled over Na/benzophenone. All reactions were performed under a dry dinitrogen atmosphere, implementing standard Schlenk procedures unless otherwise noted. UV−vis spectra were obtained with a JASCO V-670 spectrophotometer in CH_2Cl_2 solutions. Fourier transform infrared (FT-IR) spectra were measured on neat samples with a JASCO FT-IR-6300 spectrometer. Electrospray ionization mass spectrometry (ESI-MS) spectra were recorded on a Waters 600 LC/MS. Magnetic susceptibility measurements were conducted using a Johnson Matthey Mark-I magnetic susceptibility balance. Cyclic voltammograms were recorded in a 0.2 M $(n\text{-Bu})_4NPF_6$ solution (MeCN, N_2-degassed) on a CHI620A voltammetric analyzer with a glassy carbon working electrode, a platinum wire auxiliary electrode, and a $Ag/AgNO_3$ reference electrode with ferrocene used as an external reference ($E_{1/2}$ = 0.097 V, acetonitrile). The concentration of Ni(TMC) species was always 1.0 mM.

General Synthetic Procedure. To a 100 mL Schlenk flask containing [Ni(TMC)X]X (X = Cl or OTf) in THF was added the appropriate lithiated acetylide in excess, yielding an emerald-green solution, which, in some instances, became brown overnight. The reaction mixture was filtered over Celite, and the product was purified over a deactivated silica gel pad with a CH_2Cl_2/MeOH [5:1 (v/v)] eluent. The crude products were recrystallized from THF/ether.

[Ni(TMC)(C_2SiMe_3)]X ***(1)***. (a) The reaction between 0.050 g of [Ni(TMC)Cl]Cl (0.13 mmol) and 3 equiv of LiC_2SiMe_3 is given. Recrystallization from THF/ether yielded 0.026 g of [Ni(TMC)-(C_2SiMe_3)]Cl (**1a**; 0.058 mmol, 45% based on [Ni(TMC)Cl]Cl). UV−vis [λ_{max}, nm (ε M^{-1} cm^{-1})]: 669 (56), 418 (100), 327 (260). FT-IR [ν(C≡C), cm^{-1}]: 2023 (m). (b) The reaction between 0.502 g of [Ni(TMC)OTf]OTf (0.82 mmol) and 2.5 equiv of LiC_2SiMe_3 yielded 0.074 g of [Ni(TMC)C_2SiMe_3]OTf (**1b**; 0.13 mmol, 16% based on [Ni(TMC)OTf]OTf). Elem anal. Found (calcd) for [Ni(TMC)(C_2SiMe_3)]OTf: C, 42.49 (42.79); H, 7.23 (7.36); N, 9.82 (9.98).

[Ni(TMC)($C_2Si^iPr_3$)]Cl ***(2)***. The reaction between 0.206 g of [Ni(TMC)Cl]Cl (0.53 mmol) and 3 equiv of $LiC_2Si^iPr_3$ resulted in 0.222 g of **2** (0.42 mmol, 78% based on [Ni(TMC)Cl]Cl). UV−vis [λ_{max}, nm (ε, M^{-1} cm^{-1})]: 655 (74), 416 (92), 334 (330). FT-IR

DOI: 10.1021/acs.inorgchem.5b01883
Inorg. Chem. 2015, 54, 10058−10064

[ν(C≡C), cm^{-1}]: 2037 (m). Elem anal. Found (calcd) for [Ni(TMC)($C_2Si^iPr_3$)]Cl·H_2O: C, 54.59 (54.60); H, 10.12 (10.08); N, 10.15 (10.18).

[Ni(TMC)(C_2Ph)]Cl (**3**). The reaction between 0.100 g of [Ni(TMC)Cl]Cl (0.26 mmol) and 2.5 equiv of LiC_2Ph resulted in 0.071 g of **3** (0.16 mmol, 60% based on [Ni(TMC)Cl]Cl). UV−vis [λ_{max}, nm (ε, M^{-1} cm^{-1})]: 667 (65), 412 (sh), 372 (140). FT-IR [ν(C≡C), cm^{-1}]: 2093 (m). Elem anal. Found (calcd) for [Ni(TMC)C_2Ph]Cl·2H_2O: C, 54.46 (54.18); H, 8.34 (8.47); N, 11.50 (11.49).

[Ni(TMC)(C_4H)]X (**4**). (a) The reaction between 0.103 g of [Ni(TMC)Cl]Cl (0.27 mmol) and 2.1 equiv of LiC_4SiMe_3 yielded 0.065 g of [Ni(TMC)(C_4H)]Cl (**4a**; 0.16 mmol, 60% based on [Ni(TMC)Cl]Cl). Although [Ni(TMC)(C_4SiMe_3)]$^+$ was observed as a minority product in ESI-MS of the crude product in addition to $\mathbf{4}^+$ as the major product, it was no longer detected after the workup. UV−vis [λ_{max}, nm (ε, M^{-1} cm^{-1})]: 649 (76), 404 (sh), 351 (220), 324 (sh). FT-IR [ν(C≡C), cm^{-1}]: 2132 (m), 2142 (w). Elem anal. Found (calcd) for [Ni(TMC)C_4H]Cl·0.5H_2O: C, 52.83 (52.91); H, 8.49 (8.39); N, 13.71 (13.71). (b) The reaction between 0.200 g of [Ni(TMC)OTf]OTf (0.33 mmol) and 3.0 equiv of LiC_4SiMe_3 yielded 0.097 g of [Ni(TMC)(C_4H)]OTf (**4b**; 0.19 mmol, 57% based on [Ni(TMC)OTf]OTf).

Computational Details. Spin-unrestricted DFT calculations were performed with the B3LYP functional and LANL2DZ basis set, as implemented in the *Gaussian 03* program.[29] The calculations were performed using the model compounds **2′**−**4′** based on the crystal structures of **2**, **3**, and **4b**; the −$SiMe_3$ group in **2** was replaced with −H to construct the model compound **2′**. The structures **2′**−**4′** were confirmed as local minima by computing the vibrational frequencies. CASSCF/CASPT2 calculations were performed for **4′**. Scalar relativistic effects were treated through the use of the Douglas−Kroll−Hess Hamiltonian, and ANO-RCC basis sets of triple-ζ quality were employed for nickel (6s5p3d2f1g) and nitrogen (4s3p2d1f), while carbon (3s2p1d) was treated with a double-ζ basis set and hydrogen with a minimal basis set.[33] All calculations were performed using the *Molcas 7.9* software package.[34] Cholesky decomposition was used in combination with local exchange screening to reduce the cost of the two-electron integrals.[35]

X-ray Structural Analysis of 2−4. Single crystals of compound **2** suitable for X-ray structural determination were grown via slow diffusion of diethyl ether into a concentrated THF solution, and those of **3** and **4** were grown via slow diffusion of hexanes into a concentrated CH_2Cl_2 solution. X-ray diffraction data for **2**−**4** were all collected on a Rigaku Rapid II image-plate diffractometer using Cu Kα (λ = 1.54184 Å) at 200 K (Table 4), and the structure was solved using the structure solution program *PATTY* in *DIRDIF99*[36] and refined using *SHELX-07*.[37]

Table 4. Crystal Data for Compounds 2−4

	2	3	4
chemical formula	$C_{25}H_{51}N_4NiSiCl·2H_2O$	$C_{22}H_{37}N_4NiCl·1.5H_2O$	$C_{18}H_{33}N_4NiCF_3O_3S$
fw	565.99	478.75	513.27
space group	*C*2/*c*	*C*2/*c*	*Pca*2$_1$
a, Å	43.961(2)	34.999(1)	18.7849(8)
b, Å	9.0601(4)	8.4194(3)	8.3978(4)
c, Å	17.3189(7)	16.7834(5)	14.8663(5)
β, deg	111.64(3)	93.71(3)	
V, Å^3	6411.9(5)	4935.2(3)	2345.2(2)
Z	8	8	4
T, K	200	200	200
λ, Å	1.54184	1.54184	1.54184
ρ_{calcd}, g cm^{-3}	1.173	1.289	1.454
R	0.063	0.038	0.039
$R_w(F^2)$	0.180	0.105	0.096

■ ASSOCIATED CONTENT

Supporting Information

The Supporting Information is available free of charge on the ACS Publications website at DOI: 10.1021/acs.inorgchem.5b01883.

Computational details with pertinent geometric parameters for the optimized model compounds **2′**−**4′** (PDF)

X-ray crystallographic CIF files for the structural determination of **2**−**4** (CIF)

■ AUTHOR INFORMATION

Corresponding Author

*E-mail: tren@purdue.edu.

Notes

The authors declare no competing financial interest.

■ ACKNOWLEDGMENTS

The work at Purdue University is supported by the National Science Foundation (Grant CHE 1362214). We thank Professor Laura Gagliardi for her helpful suggestions.

■ REFERENCES

(1) Barefield, E.; Wagner, F. *Inorg. Chem.* **1973**, *12*, 2435−2439.
(2) Che, C. M.; Yam, V. W. W. *Adv. Inorg. Chem.* **1992**, *39*, 233−325.
(3) Barefield, E. K. *Coord. Chem. Rev.* **2010**, *254*, 1607−1627.
(4) de Visser, S. P.; Rohde, J.-U.; Lee, Y.-M.; Cho, J.; Nam, W. *Coord. Chem. Rev.* **2013**, *257*, 381−393.
(5) Ram, M. S.; Bakac, A.; Espenson, J. H. *Inorg. Chem.* **1988**, *27*, 4231−4235.
(6) Fontmorin, J. M.; He, W. Y.; Floner, D.; Fourcade, F.; Amrane, A.; Geneste, F. *Electrochim. Acta* **2014**, *137*, 511−517.
(7) Medeiros, M. J.; Neves, C. S. S.; Pereira, A. R.; Dunach, E. *Electrochim. Acta* **2011**, *56*, 4498−4503.
(8) Halcrow, M. A.; Christou, G. *Chem. Rev.* **1994**, *94*, 2421−2481.
(9) Ram, M. S.; Riordan, C. G. *J. Am. Chem. Soc.* **1995**, *117*, 2365−2366.
(10) Ram, M. S.; Riordan, C. G.; Yap, G. P. A.; Liable-Sands, L.; Rheingold, A. L.; Marchaj, A.; Norton, J. R. *J. Am. Chem. Soc.* **1997**, *119*, 1648−1655.
(11) Schenker, R.; Mock, M. T.; Kieber-Emmons, M. T.; Riordan, C. G.; Brunold, T. C. *Inorg. Chem.* **2005**, *44*, 3605−3617.
(12) (a) Ren, T. *Organometallics* **2005**, *24*, 4854−4870. (b) Cao, Z.; Xi, B.; Jodoin, D. S.; Zhang, L.; Cummings, S. P.; Gao, Y.; Tyler, S. F.; Fanwick, P. E.; Crutchley, R. J.; Ren, T. *J. Am. Chem. Soc.* **2014**, *136*, 12174−12183. (c) Xi, B.; Liu, I. P. C.; Xu, G.-L.; Choudhuri, M. M. R.; DeRosa, M. C.; Crutchley, R. J.; Ren, T. *J. Am. Chem. Soc.* **2011**, *133*, 15094−15104. (d) Ying, J.-W.; Liu, I. P.-C.; Xi, B.; Song, Y.; Campana, C.; Zuo, J.-L.; Ren, T. *Angew. Chem., Int. Ed.* **2010**, *49*, 954−957. (e) Xu, G.-L.; Zou, G.; Ni, Y.-H.; DeRosa, M. C.; Crutchley, R. J.; Ren, T. *J. Am. Chem. Soc.* **2003**, *125*, 10057−10065.
(13) Forrest, W. P.; Cao, Z.; Hambrick, H. R.; Prentice, B. M.; Fanwick, P. E.; Wagenknecht, P. S.; Ren, T. *Eur. J. Inorg. Chem.* **2012**, *2012*, 5616−5620.
(14) (a) Cao, Z.; Forrest, W. P.; Gao, Y.; Fanwick, P. E.; Zhang, Y.; Ren, T. *Inorg. Chem.* **2011**, *50*, 7364−7366. (b) Cao, Z.; Forrest, W. P.; Gao, Y.; Fanwick, P. E.; Ren, T. *Organometallics* **2012**, *31*, 6199−6206. (c) Cao, Z.; Fanwick, P. E.; Forrest, W. P.; Gao, Y.; Ren, T. *Organometallics* **2013**, *32*, 4684−4689.
(15) (a) Cook, T. D.; Fanwick, P. E.; Ren, T. *Organometallics* **2014**, *33*, 4621−4624. (b) Cook, T. D.; Natoli, S. N.; Fanwick, P. E.; Ren, T. *Organometallics* **2015**, *34*, 686−689.
(16) D'Aniello, M. J.; Barefield, E. K. *J. Am. Chem. Soc.* **1976**, *98*, 1610−1611.

DOI: 10.1021/acs.inorgchem.5b01883
Inorg. Chem. 2015, 54, 10058−10064

(17) (a) Barefield, E. K.; Freeman, G. M.; Vanderveer, D. G. *Inorg. Chem.* **1986**, *25*, 552−558. (b) Cho, J.; Kang, H. Y.; Liu, L. V.; Sarangi, R.; Solomon, E. I.; Nam, W. *Chem. Sci.* **2013**, *4*, 1502−1508.
(18) Nast, R. *Coord. Chem. Rev.* **1982**, *47*, 89−124.
(19) (a) Naulty, R. H.; Cifuentes, M. P.; Humphrey, M. G.; Houbrechts, S.; Boutton, C.; Persoons, A.; Heath, G. A.; Hockless, D. C. R.; Luther-Davies, B.; Samoc, M. *J. Chem. Soc., Dalton Trans.* **1997**, 4167−4174. (b) Whittall, I. R.; Humphrey, M. G.; Hockless, D. C. R. *Aust. J. Chem.* **1998**, *51*, 219−227. (c) Whittall, I. R.; McDonagh, A. M.; Humphrey, M. G.; Samoc, M. *Adv. Organomet. Chem.* **1998**, *42*, 291−362. (d) Whittall, I. R.; McDonagh, A. M.; Humphrey, M. G.; Samoc, M. *Adv. Organomet. Chem.* **1999**, *43*, 349−405.
(20) (a) Berry, J. F.; Cotton, F. A.; Murillo, C. A. *Dalton Trans.* **2003**, 3015−3021. (b) Cotton, F. A.; Chao, H.; Li, Z.; Murillo, C. A.; Wang, Q. S. *J. Organomet. Chem.* **2008**, *693*, 1412−1419.
(21) Butler, P.; Manning, A. R.; McAdam, C. J.; Simpson, J. *J. Organomet. Chem.* **2008**, *693*, 381−392.
(22) Wang, R. P.; Belanger-Gariepy, F.; Zargarian, D. *Organometallics* **1999**, *18*, 5548−5552.
(23) Vechorkin, O.; Godinat, A.; Scopelliti, R.; Hu, X. *Angew. Chem., Int. Ed.* **2011**, *50*, 11777−11781.
(24) Nishigaki, J.-i.; Matsumoto, T.; Tatsumi, K. *Eur. J. Inorg. Chem.* **2010**, *2010*, 5011−5017.
(25) (a) Szafert, S.; Gladysz, J. A. *Chem. Rev.* **2003**, *103*, 4175−4206. (b) Szafert, S.; Gladysz, J. A. *Chem. Rev.* **2006**, *106*, 1−33.
(26) Muetterties, E. L.; Guggenberger, L. J. *J. Am. Chem. Soc.* **1974**, *96*, 1748−1756.
(27) Addison, A. W.; Rao, T. N.; Reedijk, J.; Vanrijn, J.; Verschoor, G. C. *J. Chem. Soc., Dalton Trans.* **1984**, 1349−1356.
(28) Nishigaki, J.; Matsumoto, T.; Tatsumi, K. *Inorg. Chem.* **2012**, *51*, 5173−5187.
(29) Frisch, M. J.; Trucks, G. W.; Schlegel, H. B.; Scuseria, G. E.; Robb, M. A.; Cheeseman, J. R.; Montgomery, J. A., Jr.; Vreven, T.; Kudin, K. N.; Burant, J. C.; Millam, J. M.; Iyengar, S. S.; Tomasi, J.; Barone, V.; Mennucci, B.; Cossi, M.; Scalmani, G.; Rega, N.; Petersson, G. A.; Nakatsuji, H.; Hada, M.; Ehara, M.; Toyota, K.; Fukuda, R.; Hasegawa, J.; Ishida, M.; Nakajima, T.; Honda, Y.; Kitao, O.; Nakai, H.; Klene, M.; Li, X.; Knox, J. E.; Hratchian, H. P.; Cross, J. B.; Bakken, V.; Adamo, C.; Jaramillo, J.; Gomperts, R.; Stratmann, R. E.; Yazyev, O.; Austin, A. J.; Cammi, R.; Pomelli, C.; Ochterski, J. W.; Ayala, P. Y.; Morokuma, K.; Voth, G. A.; Salvador, P.; Dannenberg, J. J.; Zakrzewski, V. G.; Dapprich, S.; Daniels, A. D.; Strain, M. C.; Farkas, O.; Malick, D. K.; Rabuck, A. D.; Raghavachari, K.; Foresman, J. B.; Ortiz, J. V.; Cui, Q.; Baboul, A. G.; Clifford, S.; Cioslowski, J.; Stefanov, B. B.; Liu, G.; Liashenko, A.; Piskorz, P.; Komaromi, I.; Martin, R. L.; Fox, D. J.; Keith, T.; Al-Laham, M. A.; Peng, C. Y.; Nanayakkara, A.; Challacombe, M.; Gill, P. M. W.; Johnson, B.; Chen, W.; Wong, M. W.; Gonzalez, C.; Pople, J. A. *Gaussian 03*, revision D.02; Gaussian, Inc.: Wallingford, CT, 2003.
(30) Roos, B. O.; Taylor, P. R.; Siegbahn, P. *Chem. Phys.* **1980**, *48*, 157−173. Andersson, K.; Malmqvist, P. A.; Roos, B. O.; Sadlej, A. J.; Wolinski, K. *J. Phys. Chem.* **1990**, *94*, 5483−5488. Andersson, K.; Malmqvist, P. A.; Roos, B. O. *J. Chem. Phys.* **1992**, *96*, 1218−1226.
(31) Lichtenberger, D. L.; Renshaw, S. K.; Bullock, R. M. *J. Am. Chem. Soc.* **1993**, *115*, 3276−3285.
(32) By choosing a set of orbitals (denoted as the active space), the user can include all of the orbitals that are close in energy along with their corresponding electrons. Nowadays, calculations with up to 16 electrons in 16 orbitals can be performed. For example, a reasonable active space for a Ni^{II} d^8 atom would include the five d orbitals and the eight electrons, referred to as an (8,5) active space. Then, all possible ways to occupy the five orbitals with the eight electrons would be included, and the weights of each configuration are optimized along with the orbitals themselves. In this way, the contributions of each individual state can be determined, and multiple electronic configurations that lie close in energy can be treated simultaneously, ensuring that the ground state is properly defined. The orbitals lower in energy than the active space are always doubly occupied, while those that are higher are unoccupied.
(33) (a) Roos, B. O.; Lindh, R.; Malmqvist, P. A.; Veryazov, V.; Widmark, P. O. *J. Phys. Chem. A* **2005**, *109*, 6575−6579. (b) Roos, B. O.; Lindh, R.; Malmqvist, P. A.; Veryazov, V.; Widmark, P. O. *Chem. Phys. Lett.* **2005**, *409*, 295−299. (c) Roos, B. O.; Lindh, R.; Malmqvist, P. A.; Veryazov, V.; Widmark, P. O.; Borin, A. C. *J. Phys. Chem. A* **2008**, *112*, 11431−11435. (d) Hess, B. A. *Phys. Rev. A: At., Mol., Opt. Phys.* **1986**, *33*, 3742−3748.
(34) Aquilante, F.; De Vico, L.; Ferré, N.; Ghigo, G.; Malmqvist, P. A.; Neogrády, P.; Pedersen, T. B.; Pitonák, M.; Reiher, M.; Roos, B. O.; Serrano-Andrés, L.; Urban, M.; Veryazov, V.; Lindh, R. *J. Comput. Chem.* **2010**, *31*, 224−247.
(35) (a) Aquilante, F.; Gagliardi, L.; Pedersen, T. B.; Lindh, R. *J. Chem. Phys.* **2009**, *130*, 154107. (b) Aquilante, F.; Lindh, R.; Pedersen, T. B. *J. Chem. Phys.* **2008**, *129*, 034106. (c) Aquilante, F.; Malmqvist, P. A.; Pedersen, T. B.; Ghosh, A.; Roos, B. O. *J. Chem. Theory Comput.* **2008**, *4*, 694−702. (d) Aquilante, F.; Pedersen, T. B.; Lindh, R. *J. Chem. Phys.* **2007**, *126*, 194106.
(36) Beurskens, P. T.; Beurskens, G.; de Gelder, R.; Garcia-Granda, S.; Gould, R. O.; Smits, J. M. M. *The DIRDIF2008 Program System*; Crystallography Laboratory, University of Nijmegen: Nijmegen, The Netherlands, 2008.
(37) Sheldrick, G. M. *Acta Crystallogr., Sect. A: Found. Crystallogr.* **2008**, *64*, 112−122.

DOI: 10.1021/acs.inorgchem.5b01883
Inorg. Chem. 2015, 54, 10058−10064